Pharmacological Research 221 (2025) 107992

Contents lists available at ScienceDirect

Pharmacological Research

journal homepage: www.elsevier.com/locate/yphrs

K_V11.1 (hERG1)-centered macromolecular membrane complexes regulate proliferation in B cell lymphomas and constitute novel pharmacological targets

Cesare Sala [a], Jessica Iorio [a], Claudia Duranti [a], Alberto Montalbano [a], Laura Clara Grandi [b], Luciano Cascione [c,d], Markus Raderer [e], Francesco Bertoni [c,d,f], Annarosa Arcangeli [a], Andrea Becchetti [b,*]

[a] Department of Experimental and Clinical Medicine, University of Florence, Florence I-50134, Italy
[b] Department of Biotechnology and Biosciences and NeuroMI (Milan Center for Neuroscience), University of Milano-Bicocca, Milan 20126, Italy
[c] Institute of Oncology Research, Faculty of Biomedical Sciences, USI, Bellinzona, Switzerland
[d] SIB Swiss Institute of Bioinformatics, Lausanne, Switzerland
[e] Clinical Division of Oncology, Medical University of Vienna, Austria
[f] Oncology Institute of Southern Switzerland, Ente Ospedaliero Cantonale, Bellinzona, Switzerland

ARTICLE INFO

Keywords:
Clarithromycin
Diffuse large B cell lymphoma
hELK2
β1 integrin
K_V12.2
Lymphocytes
scDb-hERG1-β1

Chemical compounds studied in this article:
Cesium (PubChem CID: 5354618)
Clarithromycin (PubChem CID: 84029)
E4031 (PubChem CID: 3185)

ABSTRACT

K^+ channel modulation is essential to regulate the Ca^{2+} signals that trigger T and B lymphocyte activation. The K^+ channel complement is however deeply altered in cancer cells, as it is implicated in the neoplastic progression. We investigated the functional expression of K^+ channels in different diffuse large B cell lymphoma (DLBCL) cell lines (SU-DHL-4, WSU-DLCL2, U2932) and EBV-infected lymphocytes, as controls of normally proliferating lymphocytes. We studied the K^+ channels best characterized in lymphocytes (the voltage-gated K_V1.3 and the Ca^{2+}-activated K_{Ca}3.1) and two members of the *ether-à-go-go* (EAG) family (K_V11.1, or hERG1; K_V12.2, or hELK2) that are often overexpressed in cancer cells. All the above channel types were found in lymphoma cell lines. However, compared to normal lymphocytes, K_V1.3 and K_{Ca}3.1 tended to be substituted by EAG channels, and especially by hERG1. In all DLBCL models, cell adhesion to fibronectin stimulated the formation of the cancer-specific macromolecular complex between hERG1 and the β1 subunit of integrin receptors. No such complex was formed by hELK2. A strong reduction of lymphoma proliferation was produced when the hERG1-β1 integrin complex was disrupted by a bispecific antibody (scDb-hERG1-β1), or by the hERG1-binding macrolide antibiotic clarithromycin. Finally, in a cohort of mucosa-associated lymphoid tissue (MALT) lymphoma patients treated with clarithromycin, a trend for an improved overall survival probability was observed in patients expressing the hERG1-β1 integrin complex. Our results suggest that the hERG1-β1 integrin complex promotes lymphoma cells' proliferation. Disrupting the complex by specific targeting agents represents a new therapeutic approach to be explored.

Abbreviations: ABC, activated B cell; Akt, protein kinase B; BCL-2, B cell lymphoma 2 protein; BCL-XL, BCL extra-large; BK, big conductance KCa channels; BL, Burkitt lymphoma; BSA, bovine serum albumin; C_{CAP}, cell capacitance; CCL, chronic lymphocytic leukemia; CHO, Chinese hamster ovary; CoIP, co-immunoprecipitation; CRAC, calcium release activated channels; DLBCL, diffuse large B cell lymphoma; EAG, *ether-à-go-go*; EBV, Epstein-Barr virus; E_K, K^+ equilibrium potential; FBS, fetal bovine serum; FL, follicular lymphoma; *GAPDH*, glyceraldehyde 3-phosphate gene; GCB, germinal center B cell type; hELK2, human EAG-like channel type 2; hERG1, human EAG-related channel type 1; HIF-1a, hypoxia-inducible factor 1a; IF, immunofluorescence; IHC, immunohistochemistry; KCNE1-E3, accessory subunits of hERG1; Kir, inward-rectifier K^+ channel; MALT, mucosa-associated lymphoid tissue; MCL, mantle cell lymphoma; MZL, marginal cell lymphoma; NFAT, nuclear factor of activated T cells; PBS, phosphate-buffered saline; PI3K, phosphatidylinositol 3-kinase; PMBCL, primary mediastinal large B cell lymphoma; scDb-hERG1-β1, bispecific antibody linking hERG1 and the β1 integrin subunit; V_H, holding potential; $V_{0.5}$, half-activation potential; V_m, transmembrane potential; V_{REST}, resting V_m.

* Correspondence to: Department of Biotechnology and Biosciences, University of Milano-Bicocca, Piazza della Scienza 2, Milan 20126, Italy.
E-mail addresses: cesare.sala@unifi.it (C. Sala), jessica.iorio@unifi.it (J. Iorio), claudia.duranti@unifi.it (C. Duranti), a.montalbano@lab.gea.green (A. Montalbano), laura.grandi@unimib.it (L.C. Grandi), luciano.cascione@ior.usi.ch (L. Cascione), markus.raderer@meduniwien.ac.at (M. Raderer), francesco.bertoni@ior.usi.ch (F. Bertoni), annarosa.arcangeli@unifi.it (A. Arcangeli), andrea.becchetti@unimib.it (A. Becchetti).

https://doi.org/10.1016/j.phrs.2025.107992
Received 17 July 2025; Received in revised form 29 September 2025; Accepted 10 October 2025
Available online 11 October 2025

1. Introduction

Lymphocytes express a fine-tuned network of ion channels and transporters that modulate the cytoplasmic concentrations of divalent cations such as Ca^{2+}, Mg^{2+}, and Zn^{2+}. These act as second messengers, regulating lymphocyte differentiation as well as effector functions, including cytokine production and cytotoxicity [1]. Classic work showed that Ca^{2+} exerts a critical messenger function during T lymphocyte activation by antigen-presenting cells. The process is mediated by the CD3 membrane complex, which stimulates phospholipase Cγ, and thus production of inositol 1,4,5-trisphosphate (IP_3). The ensuing release of calcium from endoplasmic reticulum causes further elevation of cytosolic Ca^{2+}, because of activation of Calcium Release Activated Channels (CRAC) on the plasma membrane. Overall, the calcium signal promotes T cell proliferation through a Ca^{2+}/calmodulin dependent activation of calcineurin, whose phosphatase action promotes transcription of the Nuclear Factor of Activated T cells (NFAT; [1–3]).

Cytoplasmic calcium elevation can be fostered by increasing the transmembrane driving force for Ca^{2+}, through K^+ channel-dependent membrane hyperpolarization [1,3,4]. The best-characterized K^+ channels in lymphocytes are the voltage-activated $K_V1.3$ and the Ca^{2+}-activated $K_{Ca}3.1$, respectively encoded by *KCNA3* and *KCNN4*. $K_V1.3$ is a homotetramer of α-subunits belonging to the voltage-dependent channel superfamily [5,6]. $K_{Ca}3.1$ is an intermediate conductance Ca^{2+}-activated K^+ channel whose carboxy-terminal domain is constitutively bound to calmodulin and stimulates channel opening on cytosolic calcium elevation [7]. $K_{Ca}3.1$ engagement also requires phosphatidylinositol-3 phosphate (PI(3)P)-dependent histidine phosphorylation, following lymphocyte activation [1]. In T cells, $K_V1.3$-dependent hyperpolarization facilitates Ca^{2+} influx through CRAC channels [3] and other pathways [8]. In turn, cytosolic Ca^{2+} increase and IP_3 production exert positive feedback that sustains membrane hyperpolarization, by stimulating $K_{Ca}3.1$ [1,2]. The role of $K_V1.3$ and $K_{Ca}3.1$ in Ca^{2+} signaling is controlled by their expression levels, which vary among lymphocyte subsets as a function of lymphocyte development and state of activation [3,9–11]. Although evidence is less extensive than for T cells, several lines of evidence indicate that analogous mechanisms are operant in B lymphocytes [12].

Despite their well-characterized physiological role in lymphocytes, the expression and function of K^+ channels during the tumorigenic transformation of lymphocytes into lymphomas are unknown. The neoplastic transformation entails a profound modification of a cell's physiology and interaction with the extracellular environment, which requires a wide restructuring of the plasma membrane transport machinery. As a consequence, ion channels and transporters are often found to be aberrantly expressed in human cancers. Hence, they are increasingly recognized as useful cancer biomarkers [13], and the related gene expression profile has been proven to be a powerful clinical tool in several types of cancers, including lymphomas [14]. Specifically, in lymphocyte-derived tumors, such as B cell precursor acute lymphoblastic leukemia, K^+ channels are often overexpressed [15,16] and sustain the development of chemoresistance [17].

Diffuse large B cell lymphoma (DLBCL) is the most common lymphoma type [18,19]. It is an aggressive disease which may represent the histologic transformation of indolent lymphomas, such as follicular lymphoma (FL; [20]). In FL, we recently showed an altered K^+ channel expression, leading to a progressive decrease in excitability and a metabolic shift towards oxidative metabolism [14]. $K_V1.3$ and $K_{Ca}3.1$ were replaced by inwardly rectifying K^+ channels (Kir) and Big conductance K_{Ca} channels (BK) (*KCNJ8*, *KCNJ10*, *KCNJ5*, *KCNMA1)* [14]. As in other tumors, the different K^+ channel complement in lymphoma and lymphocytes, accompanied by distinct physiological roles of the lymphoma-specific channels, offers the possibility of selective K^+ channel targeting for pharmacological treatment of lymphomas [2,21]. This approach could be further facilitated by the differential expression of K^+ channel subtypes in distinct cell types, which allows selective targeting of lymphocyte/lymphoma subsets.

The human *ether-à-go-go (eag)* genes, encoding a subfamily of voltage-gated K^+ channels, are also implicated in neoplasia. In particular, the *eag-related gene 1* (or *KCNH2*, encoding the $K_V11.1$ channel, also known as hERG1, in humans) is abnormally overexpressed in cancer cells of epithelial, muscle, and nervous tissue origin [22,23]. HERG1 is also up-regulated in neoplastic hematopoietic cells, and blocking hERG1 currents reduces cell proliferation [24]. In these cancers, hERG1 is strictly bound to the β1 subunit of integrin receptors, thus participating in a supramolecular structure that can recruit other membrane receptors and transport proteins, to promote cancer cell growth and invasiveness [25–27]. Such a macromolecular complex is specific of cancer cells, as in non-neoplastic tissue hERG1 preferentially associates with its classic accessory subunits [26]. Studies on the biophysically similar $K_V12.2$ (or hELK2, encoded by the *eag-like gene 2*, or *KCNH3*) are less extensive, but evidence about its implication in tumors is growing [28–31].

Based on these premises, we studied the expression pattern of K^+ channels in germinal center B cell type (GCB) and activated B cell (ABC) DLBCL cell lines, using Epstein-Barr virus (EBV)-infected B lymphocytes as control. Moreover, we studied the K^+ channel implication in lymphoma proliferation, with special focus on the role exerted by the cancer-specific complex that hERG1 forms with the β1 subunit of integrin adhesion receptors.

2. Materials and methods

Unless otherwise indicated, chemicals were purchased from Sigma-Aldrich (Merck KGaA, Darmstadt, Germany).

2.1. Human lymphoma cell lines and other cell cultures

EBV-infected B lymphocytes (CD19 +) [17] were maintained in RPMI 1640 medium (Euroclone, Milan, Italy) supplemented with 2 mM glutamine, 10 % fetal bovine serum (FBS; HyClone), 1 μM hydrocortisone, 100 U/mL penicillin (Euroclone), and 100 μg/mL streptomycin (Euroclone). The DLBCL cell lines SU-DHL-4 (DLBCL-GCB), WSU-DLCL2 (DLBCL-GCB) and U2932 (DLBCL-ABC) were cultured in RPMI 1640 medium supplemented with 2 mM L-glutamine, 10 % bovine calf serum (HyClone), 100 U/mL penicillin and 100 μg/mL streptomycin. All the cell lines used in the present study were routinely screened for Mycoplasma contamination, and only Mycoplasma negative cells were used. HEK293, HCT116, HeLa, CHO cells were routinely cultured at 37 °C with 5 % CO_2 in a humidified atmosphere, in RPMI 1640 medium (HCT116) or in Dulbecco's modified Eagle's Medium (DMEM; Euroclone) (HEK293 and HeLa), or Ham F12 (CHO) supplemented with 2 % L-Glut and 10 % FBS (Euroclone). HEK 293 cells expressing the hERG1 construct (HEK 293 hERG1) were prepared as previously described [26] and maintained in complete culture medium supplemented with 0.8 mg/mL of Geneticin (G418, Thermo Fisher Scientific, Waltham, MA).

For Real-time PCR, Western blot and proliferation experiments, SU-DHL-4, WSU-DLCL2, U2932, EBV-infected B lymphocytes, CHO (-) CHO-hERG1, CHO-Kv1.3, HeLa and HCT116 have been analyzed after 2 weeks in culture, at 1×10^6 cells/mL or 80 % of confluency for adherent cells. For co-immunoprecipitation (Co-IP) and immunofluorescence (IF) experiments, SU-DHL-4, WSU-DLCL2, U2932, EBV-infected B lymphocytes, HEK 293 and HEK 293 hERG1 cells were starved overnight by culturing them in serum-free-BSA (bovine serum albumin) medium, containing 250 mg/mL of heat inactivated BSA (Fraction V; Euroclone). Next, cells were seeded on culture dishes/glass slides preliminarly coated with fibronectin (human plasma) diluted in sterile PBS (Euroclone) at 5 μg/cm^2 concentration. The culture surface was coated with a minimal volume. The dishes were left air-drying for 1 h at room temperature before introducing cells and medium. Cells resuspended in serum-free-BSA medium, were added at different concentrations

depending on the type of experiment to be performed.

2.2. RNA-Seq data

RNA expression values of the genes of interest were extracted from the dataset GSE221770, previously produced via total-RNA-Seq [32].

2.3. RNA extraction, cDNA retrotranscription and real-time (RT) PCR

For total RNA extraction, we used Trizol (Invitrogen, Carlsbad, CA), following manufacturer's instructions. Only the samples displaying a RIN (RNA integrity number) > 6 at the Agilent 2100 Bioanalyzer (Agilent Technologies, Santa Clara, CA) were further processed for gene expression analysis. We retrotranscribed 1 μg RNA using SuperScript IV (Invitrogen, Carlsbad, CA), according to manufacturer's indications. PCR was performed as in [25]. Primers are reported in Supplementary Table 1.

2.4. Western blotting and Co-IP

Protein extraction and Western blotting were performed as described in [26]. Cells starved overnight and collected were seeded on fibronectin-coated 100 mm Petri dishes at 1.5/1.75 × 106 cells/mL in 5 mL of serum-free-BSA medium. Antibodies used and dilutions are reported in Supplementary Table 2.

For Co-IP experiments, cells were seeded and incubated on fibronectin for 90 min. Treatments were performed by adding CsCl (5 mM), E4031 (30 μM) (Tocris, Bioscence, Bristol, UK), scDb-hERG1-β1 (100 μg/mL) (MCK Therapeutics, Pistoia, Italy), or clarithromycin (160 μM), during the 90 min of incubation. Cells were gently collected by mild scraping and resuspended in ice-cold phosphate-buffered saline (PBS). Protein extraction, quantification, and total lysate incubation with protein A/G agarose beads (Santa Cruz Biotechnology, Texas, USA) were performed as previously reported [26]. The lysis buffer contained: NP40 (150 mM), NaCl (150 mM), Tris-HCl pH 8 (50 mM), EDTA pH 8 (5 mM), NaF (10 mM), $Na_4P_2O_7$ (10 mM), Na_3VO_4 (0.4 mM), and protease inhibitor cocktail (complete Mini-Roche, Roche Diagnostics, Mannheim, Germany). All the procedures were performed maintaining samples on ice. Lysates were centrifuged at 13000 g for 10 min, at 4°C. Supernatants were then collected and assayed for protein concentration using Bradford protein assay (Bio-Rad, Hercules, CA), following manufacturer's instructions. Samples for Co-IP (1.5 mg of protein) were subjected to a pre-clearing step, consisting of a 2 h incubation at 4°C under rotation with Protein A/G Plus-Agarose beads, following manufacturer's instructions. Thereafter, cell lysates were immunoprecipitated with TS2/16 antibody at the concentration indicated in Supplementary Table 2 by overnight incubation at 4°C under gentle rotation. Beads were washed three times with PBS and the bound protein component was eluted by boiling the samples in Laemmli buffer for 5 min at 95°C. The obtained samples were run on a 7.5 % polyacrylamide gel for 1 h at 100 V, in Tris-glycine-SDS running buffer (Bio-Rad). Gels semi-dry blotting on PVDF membranes was performed with Turbo blot (Bio--Rad) using the "HIGH MW" program (1.3 A, 25 V, for 10 min). Membranes were incubated 2 h at room temperature with 0.1 % Tween 20 in PBS (PBS-T) containing 5 % BSA. Blots were then incubated overnight at 4°C with primary antibodies against hERG1, β1 integrin or hELK2 at the concentrations indicated in Supplementary table 2. Membranes were then washed three times with PBS-T and incubated with IRDYe 800 CW anti-mouse and anti-rabbit secondary antibodies for 45 min at room temperature, at the concentration indicated in Supplementary Table 2. After three washes with PBS-T, immunoreactivity was determined by LI-COR Odyssey Scanner apparatus (LI-COR Biosciences, Lincoln, NE). For membranes stripping the ReBlot Western blot recycling kit (Merck Millipore, Burlington, MA) was routinely used according to manufacturer's instructions. For Western blot experiments and Co-IP inputs signal detection, proteins were extracted and quantified as previously described. Fifty μg of protein were assayed for hERG1, $K_{Ca}3.1$, $K_V1,3$, hELK2, β1 integrin and Tubulin, samples were denatured in 4X Laemmli buffer at 95°C for 5 min and then run by Sodium dodecyl Sulfate-Poly-Acrylamide Gel Electrophoresis (SDS-PAGE), using 7.5 % polyacrylamide gels. Blotting was performed using the TurboBlotTM "MIXED MW" program (1.3 A, 25 V, for 7 min). Membranes were then washed three times with PBS-T and incubated with IRDYe 800 CW anti-mouse and anti-rabbit secondary antibodies for 45 min at room temperature at the concentration indicated in Supplementary Table 2.

2.5. Densitometric analysis

Densitometric analysis was performed using ImageJ software (ImageJ v.1.38, U.S. National Institutes of Health) on three different scans following background subtraction. Results were obtained from at least three different independent experiments. The hERG1/β1 integrin complex was quantified as reported [26]. In brief, the densitometric signal for the co-immunoprecipitated protein (hERG1) was divided by the signal of the protein used for immunoprecipitation (β1 integrin). The result was then normalized to the signal of the corresponding protein in the total lysate (input hERG1). The resulting value is indicated as "hERG1/β1 integrin complex" throughout the manuscript and in the figures.

2.6. Patch-clamp recording

On the experiment day, cells were centrifuged and resuspended in an RPMI-1640 serum-free medium and then kept at 37°C for at least 1 h to promote cell adhesion to the plate surface. Before recording, cells were identified at 40x magnification with a Nikon Eclipse TE300 microscope (Nikon Instruments Spa, Campi Bisenzio, Italy) equipped with a Photometrics CoolSNAP CF camera (Teledyne Photometrics, Tucson, AZ). Membrane currents were recorded at room temperature (~25°C) in the whole-cell configuration of the patch-clamp technique. Patch pipettes were pulled from borosilicate glass capillary tubes, and their resistance was 4–5 MΩ. The pipette capacitance was manually compensated up to 90–95 % after reaching a stable gigaseal (≥4 GΩ). The Multiclamp 700 A equipment and pCLAMP 9.2 software (Molecular Devices, Sunnyvale, California, USA) were used for stimulation and recording. V_{REST} was measured in open-circuit condition (I=0 mode), and cell capacitance (C_{CAP}) was measured with the same extracellular solution. The recordings were low-pass filtered at 3 kHz and digitally sampled at 25 kHz.

The hERG1 and hELK2 currents were studied as tail currents at −120 mV (for 1 s), after conditioning voltage steps ranging from + 20 mV to −100 mV (10 mV steps; 5 s duration). Holding potential (V_H) was 0 mV. In some experiments, to reduce cell stress, the conditioning potential ranged from 0 mV to −100 mV (20 mV steps). The main extracellular solution ($E_K = -80$ mV) contained (mM): 130 NaCl, 5 KCl, 2 $CaCl_2$, 2 $MgCl_2$, 10 Hepes–NaOH, and 5 Glucose 5, pH 7.4 (adjusted with NaOH). The hERG1 and hELK2 currents were studied using an extracellular solution with high K^+, to increase the driving force for K^+. In this case ($E_K = -30$ mV), NaCl (95 mM) was partially substituted by KCl (40 mM). The patch-clamp pipette contained: 130 K^+-aspartate, 10 NaCl, 4 $CaCl_2$, 2 $MgCl_2$, 10 Hepes-NaOH, 10 EGTA, pH 7.3. To specifically block hERG1 currents, E4031 (1 μM) was applied for 1 min. The resulting current was then subtracted from the current measured in control conditions to evaluate the net hERG1 current. This procedure allows to also distinguish hELK2 currents, which are biophysically similar to hERG1, but are not sensitive to E4031 and other hERG1 blockers [28]. Activation curves were obtained by plotting normalized peak tail currents, as a function of the conditioning V_m. Data points in Fig. 2B were fit (with Levenberg-Marquardt procedure) to a Boltzmann function of the form:

$$\frac{I}{I_{max}} = \frac{1}{1 + \exp\left(-\frac{V_m - V_{0.5}}{n}\right)}$$

where I is the peak tail current measured at −120 mV after a given conditioning V_m, I_{max} is the maximal peak tail current, $V_{0.5}$ is the voltage of half-maximal activation, V_m is the applied membrane potential and n is a slope factor measuring the apparent gating charge.

2.7. Cell proliferation assay

From each cell model, 5×10^3 cells/well in 96-well plates were seeded in complete media. Clarithromycin (160 μM; i.e.,120 μg/mL) or scDb-hERG1-β1 (50 μg/mL; i.e., 0.735 μM) were added from the day of cell seeding. scDb-hERG1-β1 was freshly added every 24 h. Viable cell counts were conducted every 24 h for four days. Living cells were identified as cells negative to trypan blue staining, in control and treatment condition.

2.8. Immunofluorescence (IF)

Following non-adherent cell removal, cells were fixed with 4 % paraformaldehyde for 15 min and then permeabilized with Triton X-100 (0.1 % for 30 min). Following a 2 h blocking step in PBS with 10 % BSA, slides underwent an additional 2 h incubation period with scDb-hERG1-β1 (final concentration of 20 μg/mL), succeeded by 1 h incubation with anti-6xHis and next 1 h with anti-mouse Alexa Fluor 488. Nuclei were stained with Hoechst (1:1000 in PBS, 10 min). Imaging was performed using a confocal microscope (Nikon TE2000). Primary and secondary antibodies are detailed in Supplementary Table 2.

2.9. Immunohistochemistry (IHC)

Twenty cases of extranodal marginal zone lymphoma (MZL) of the mucosa-associated lymphoid tissue (MALT lymphoma) (6 males, 14 females; mean age of 69 years, range 36–84 years) were obtained from the Clinical Division of Oncology (Medical University of Vienna, Austria). Clinical data were obtained from the internal database of the Clinical Division of Oncology (Medical University of Vienna, Austria), in compliance with the regulations of the country in which the study was carried out, and are shown in Supplementary Table 3.

A commercially available lymphoma tissue microarray containing 92 primary DLBCL (59 males, 33 females; mean age of 46 years, range 6–83 years) was obtained from TissueArray (LY2083 BioMax).

Formalin-fixed, paraffin-embedded samples were analysed for the expression of the hERG1-β1 integrin complex. IHC was carried out on 7 μm sections on positively charged slides. After dewaxing and rehydrating the sections, endogenous peroxidases were blocked with a 1 % H_2O_2 solution in PBS. Subsequently, antigen retrieval was performed by treatment with proteinase K (5 μg/mL) in PBS at 37 °C for 5 min. Sections were incubated with a solution of FBS (1:50 in PBS) for 5 min at room temperature. Incubation with the primary scDb-hERG1-β1 (final concentration of 20 μg/mL) was carried out overnight at 4 °C. Next, sections were incubated with anti-6xHis 1:250 for 90 min at room temperature. Finally, immunostaining was performed with a commercially available kit (PicTure max kit; Invitrogen, Invitrogen. Carlsbad, CA) according to the manufacturer's instructions, and nuclei were counterstained with Mayer's hematoxylin. Immunohistochemistry slides were scored by two independent operators (C.S. and J.I.). Samples were considered positive when the percentage of stained cells was higher than 1 %.

2.10. Statistics

Unless otherwise stated, categorical variables are presented with counts and proportions, whereas the continuous ones are presented as mean values ± standard error of the mean (s.e.m.), with n indicating the number of independent experiments. Statistical analysis was performed using GraphPad Prism v8.0 (GraphPad Software, San Diego, California, USA) or OriginPro 2023 (OriginLab Corporation, Northampton, MA, USA). For comparisons between two groups, we applied two-tailed paired Student's *t*-test, after checking normality (Shapiro-Wilk test) and variance homogeneity (F-test). In case of non-normal distributions, we applied the Wilcoxon Sign Rank test. Multiple comparisons of Western blot, Co-IP, and proliferation experiments were carried out with one-way ANOVA, followed by Bonferroni's post hoc test. Preliminarily, normality of data was checked with the Shapiro-Wilk test, and variance homogeneity (Brown-Forsythe test). The derived p-values (p) are indicated as * ($p \leq 0.05$), ** ($p \leq 0.01$), *** ($p \leq 0.001$), **** ($p \leq 0.0001$). The IHC correlations were analyzed with Fisher's exact test. Differences in mean survival between groups, as represented in Kaplan–Meier survival curves, were analyzed using the log-rank test, also performed with GraphPad Prism.

3. Results

3.1. K^+ channels in lymphoma cells: analysis of transcripts and proteins

Taking advantage of a previously obtained RNA-Seq dataset [32], we first examined the RNA expression of different K^+ channel encoding genes (*KCNA3, KCNN4*, *KCNH1, KCNH2, KCNH3, KCNH6* and *KCNH7*) in cell lines derived from GCB and ABC DLBCL, Burkitt Lymphoma (BL), primary mediastinal large B cell lymphoma (PMBCL), mantle cell lymphoma (MCL), MZL and chronic lymphocytic leukemia (CLL) (Fig. 1A; Supplementary Fig. 1). Transcriptomic analysis showed a negligible expression of *KCNH1, KCNH6* and *KCNH7*. In contrast, widespread expression was observed for *KCNA3* and *KCNN4,* in agreement with the well-known implication of $K_{Ca}3.1$ and $K_V1.3$ in lymphocyte activation. Significant expression was also detected for the members of the *KCNH*/EAG family *KCNH2* (encoding hERG1) and, to a lesser extent, *KCNH3* (hELK2). The transcript amounts of individual channel types, however, differed among the analyzed lymphoma cell lines. In particular, *KCNH2* and *KCNH3* transcripts were detected prevalently in DLBCL, MZL, and MCL (Fig. 1A). In particular, the three DLBCL lymphoma cell lines, WSU-DLCL2, SU-DHL-4 (both GCB) and U2932 (ABC) highly expressed *KCNH2,* albeit at different levels. In these cells, significant amounts of *KCNH3* transcript were observed in U2932 and WSU-DLCL2. On the other hand, *KCNA3* was expressed only (at high levels) in the ABC DLBCL cell line U2932, and *KCNN4* was expressed in all the DLBCL cell lines, with SU-DHL-4 showing the highest levels (Fig. 1B). To better quantify the expression of the different genes, the RNAseq results were followed up by applying RT PCR on the three DLBCL cell lines SU-DHL-4, WSU-DLCL2, U2932 as well as on EBV-infected lymphocytes, which are immortalized activated B lymphocytes usually employed as a model of proliferating normal B lymphocytes [16]. As positive controls for the different RT-PCRs, we used (a) Chinese hamster ovary (CHO) cells stably expressing hERG1 or $K_V1.3$ [33] for *KCNH2* and *KCNA3*, respectively; (b) the HeLa cervical cancer cell line for *KCNH3* and (c) the HCT116 colorectal cancer cell line for *KCNN4*. WT CHO cells were used as negative controls, as they express very low K^+ channel levels [33]. The RT-PCR results mirrored the K^+ channel distribution pattern evinced by the RNA-seq analysis. Moreover, they point to *KCNN4* and *KCNA3* downregulation in all DLBCL lines, compared to EBV-infected lymphocytes, whereas the opposite was observed for *KCNH2* in all the DLBCL cell lines and for *KCNH3* in the ABC DLBCL cell line U2932 (Fig. 1**C**).

We next evaluated the expression levels of the corresponding proteins. $K_V1.3$, $K_{Ca}3.1$ and hELK2 were detected in all the lymphoma cell lines, but at significantly lower amounts compared to EBV-infected lymphocytes. hERG1 displayed higher expression in all the lymphoma cell lines compared to the EBV-infected lymphocyte controls. Particularly high hERG1 amounts were detected in the ABC DLBCL U2932 cell line (Fig. 1**D** and the corresponding densitometric analysis in Fig. 1E). Overall, the proteomic characterization in SU-DHL-4, WSU-DLCL2, and U2932 was consistent with the transcriptomic data.

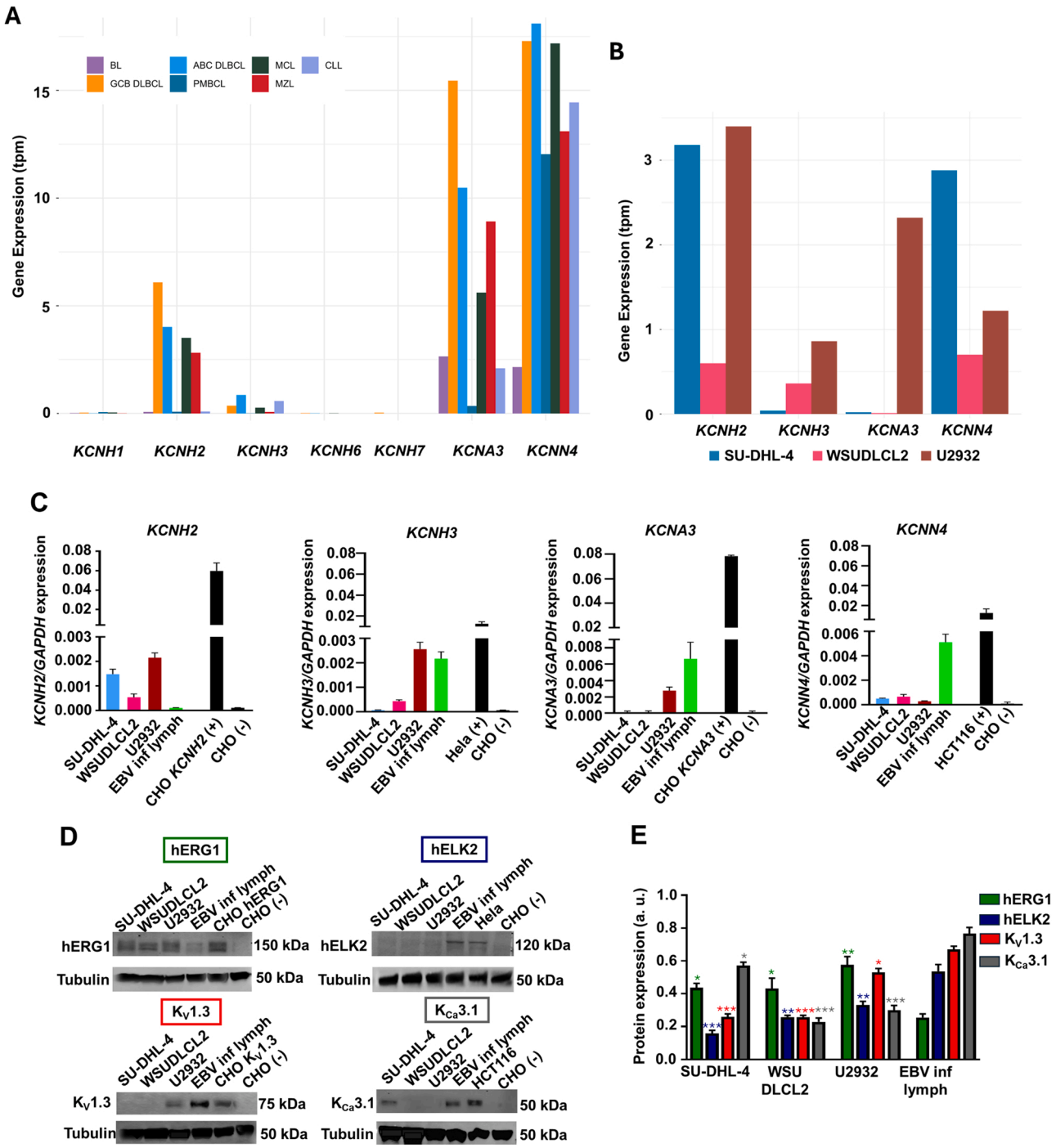

Fig. 1. Expression of K^+ channels in different lymphoma cell lines. (A) RNAseq analysis showing the transcription level, expressed in transcripts per million (TPM) of *KCNH1, KCNH2, KCNH3, KCNH6, KCNH7, KCNA3, KCNN4* in cell lines of different lymphoma subtypes: BL, DLBCL (GCB and ABC), PMBCL, MCL, MZL, and CLL. (B) Detailed transcription level of *KCNH2, KCNH3, KCNA3,* and *KCNN4* in the SU-DHL-4, WSU-DLCL2, and U2932 DLBCL lines. (C) Expression levels of *KCNH2, KCNH3, KCNA3,* and *KCNN4* analyzed by quantitative RT PCR performed on cDNA of EBV-infected B lymphocytes (EBV inf lymph) and of the SU-DHL-4, WSU-DLCL2, and U2932 DLBCL lines. CHO WT, CHO hERG1, CHO $K_V1.3$, HCT116, and HeLa were used as positive (+) and negative (-) controls. The expression levels were normalized to that of the Glyceraldehyde 3-Phosphate gene (*GAPDH*). (D) Representative Western Blot of hERG1, hELK2, $K_V1.3$ and $K_{Ca}3.1$ proteins in the indicated DLBCL. (E) Tubulin relative expression of the different K^+ channels in the different DLBCL cell lines. Statistical significance (one-way ANOVA) for each channel expression is reported in comparison to EBV Inf Lymph. Data are averages of 3 experiments.

3.2. K^+ channels in lymphoma cell lines: electrophysiological analysis

The K^+ currents in our DLBCL cell lines were next characterized by applying the whole-cell configuration of the patch-clamp method. We had previously studied $K_V1.3$ and $K_{Ca}3.1$ in the selected lymphoma models by the same method (data available in the data accessibility section). A significant $K_V1.3$ current was only observed in SU-DHL-4, whereas no appreciable $K_{Ca}3.1$ current was observed in any of the analyzed DLBCL cell lines [34]. These results are in overall agreement with the proteomic data (Fig. 1E), except for SU-DHL-4 cells, which displayed a higher $K_{Ca}3.1$ protein expression, compared to the other cell lines. The possible reasons for such a discrepancy are discussed in

Section 4.1.

Here, we focused on hERG1 currents, which were measured as inward 'tail' currents at −120 mV, following 5 s conditioning voltage steps ranging from 0 to −100 mV, with $V_H = 0$ (Fig. 2A, right panel). The maximal channel activation is obtained by the conditioning step at 0 mV, which is followed by inactivation. On hyperpolarizing at −120 mV, inactivation is quickly removed, allowing the measurement of the hERG1 current before the slower deactivation (closure) occurs [28,35]. Conditioning steps of 5 s duration allow reaching steady state for the kinetic transitions of hELK2 and to obtain a reasonable approximation to the steady state for hERG1 [28,35]. In EBV-infected lymphocytes, about half of the tested cells showed small inward currents at −120 mV. An example is shown in Fig. 2A (left panel). In these cells, the average maximal current was −46.25 ± 18 pA (n = 4), which was not completely blocked by 1 μM E4031 (Fig. 2A, middle panel). This was consistent with the concomitant expression of hELK2 (*KCNH3*) in EBV-infected lymphocytes (Fig. 1C), which is known to be insensitive to the common hERG1 blockers, including E4031 [28]. U2932, WSU-DLCL2, and SU-DHL-4 generally displayed considerably higher current amplitudes at −120 mV, compared to the EBV-infected controls, in agreement with the higher *KCNH2* expression. Examples of tail currents recorded from these cell lines are shown, respectively, in Figs. 2B, 2C and 2D. As expected, these currents were only partially sensitive to E4031 (middle panels), but almost fully blocked by the broad K^+ channel blocker Cs^+ (5 mM; an example is given for U2932 cells; middle panel of Fig. 2B). These results are in line with the mixed hERG1/hELK2 expression suggested by the transcriptomic and biochemical results. The smallest effect of E4031 (~20 %, on average) was observed in SU-DHL-4

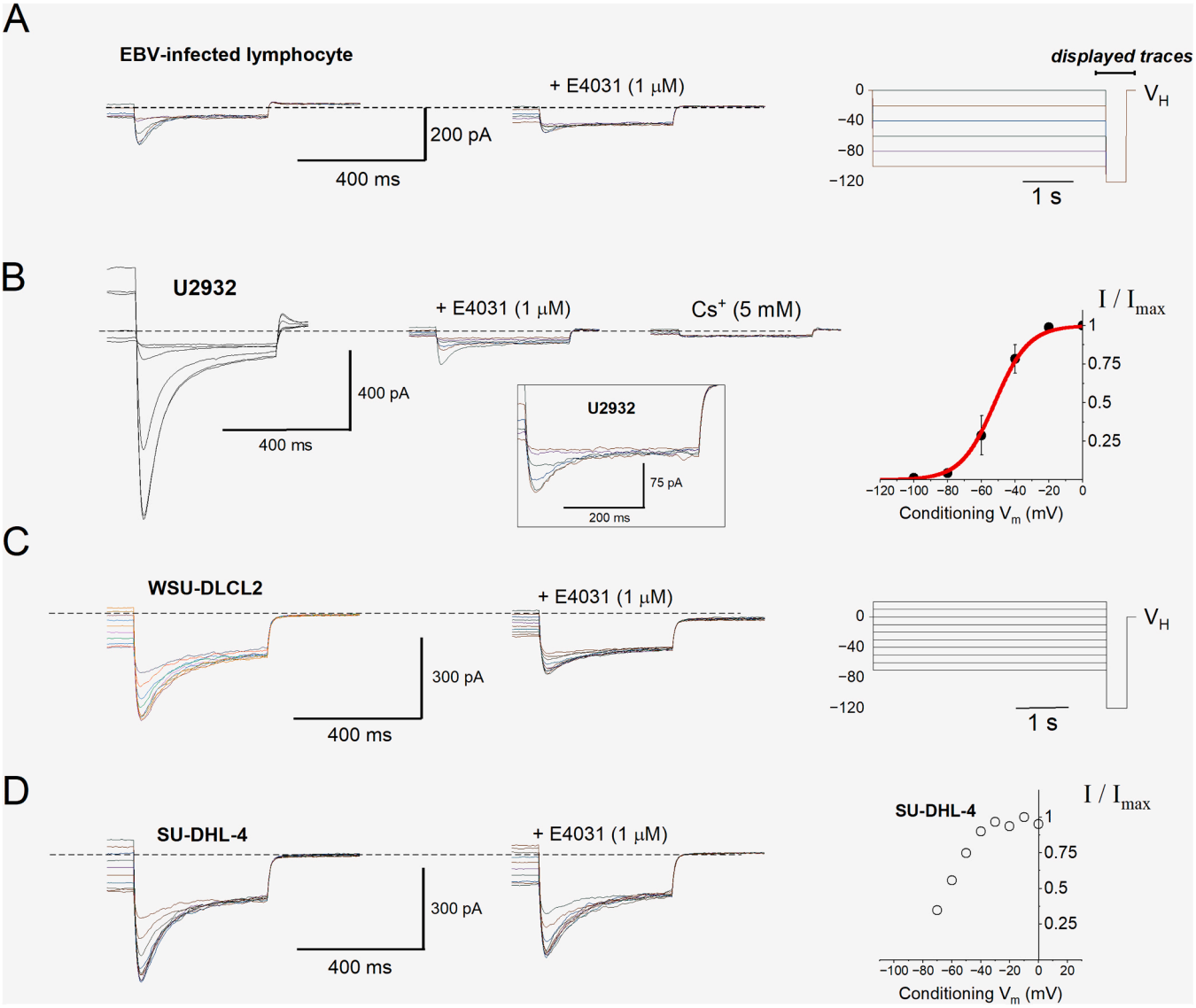

Fig. 2. EAG-type K^+ currents in lymphoma cells. (A) Representative tail current traces at −120 mV, from an EBV-infected lymphocyte. Left panel: control conditions. Middle panel: in the presence of E4031. Right panel: stimulation protocol; tail currents were recorded for 0.5 s at −120 mV, after 5 s conditioning voltage steps (-100–0 mV; $V_H = 0$ mV). The bar on top of the stimulus protocol indicates the time segment corresponding to the displayed current traces. (B) Left and middle panels: same as (A), for U2932 cells, except that the effect of 5 mM Cs^+ is also shown, for comparison with E4031. This cell's currents had especially high-amplitude, and allow to best convey the residual currents after blockade with E4031. Inset: tail current traces at −120 mV from a U2932 cell displaying more typical tail current amplitudes. The rightmost panel reports the activation curve for E4031-sensitive currents. Data points are average normalized peak tail currents, from 4 experiments in the same cell batch. Data were fitted to a Boltzmann function (see Section 2.7), with $V_{0.5}$ = -52 mV ± $8.7 \cdot 10^{-16}$, and n = 10 ± $7.65 \cdot 10^{-16}$. (C) Representative tail current traces for WSU-DLCL2, in presence or absence of E4031, as indicated. Stimulus was as in (A), except that the conditioning voltage steps ranged from −70 mV to + 20 mV (right panel). (D) Same as (C), for SU-DHL-4 cells. The right panel shows the activation curve in presence of E4031 (reflecting the putative pure hELK2 current) for the same cell.

(control: −143 ± 35.53 pA; E4031: −116.4 ± 33.26 pA; p = 0.005 with paired *t*-test, n = 7). In WSU-DLCL2 cells, the peak tail current reduction caused by E4031 application was ~60 % (control: −138.1 ± 37.34 pA; E4031: −81.3 ± 21.88 pA; p = 0.02 with paired *t*-test, n = 7). In U2932, the tail current was also mostly carried by hERG1, as approximately 80 %, on average, was blocked by E4031 (control: 190.8 ± 65.3 pA, median 75.5 pA; E4031: 37.2 ± 10.3, median 17.5; p < 0.0001 with Wilcoxon test, n = 14). The activation curve for hERG1 in U2932 cells (i.e., E4031-sensitive currents) is shown in Fig. 2B (right panel). Because of the comparatively high expression of hELK2 currents in SU-DHL-4 and WSU-DLCL2, in a fraction of cells from these lines we applied conditioning voltages in 10 mV steps (up to +20 mV), to better sample the membrane potential (V_m) region between the cell's resting potential (V_{REST}) and the activation plateau. Examples are shown in Figs. 2C and 2D. The right panel of Fig. 2D shows the activation curve of the putative hELK2 current (i.e., the current recorded in the presence of E4031), in the displayed SU-DHL-4 cell. Overall, the V_m of half-activation ($V_{0.5}$) was generally < -50 mV, in lymphoma cell lines, irrespective of the balance of hERG1 and hELK2. This is consistent with a V_{REST} close to −50 mV, in the lymphoma cells expressing detectable EAG-type currents (Table 1). The measured $V_{0.5}$ values depend on V_H and the duration of the conditioning voltage steps [35]. For hERG1, $V_{0.5}$ values around −50 are in broad agreement with those reported in immortalized and cancer cells, after stimulation with a voltage protocol similar to the one used here (V_H = 0 mV; 5 s conditioning steps; e.g., [17,22,35]). In contrast, for hELK2, the activation $V_{0.5}$ was more negative than previously reported in glioma [28], the only tumor type in which such an analysis is available, to the best of our knowledge. One possible explanation is that, in lymphoma cell lines, a higher fraction of hELK2 channels is associated with accessory subunits such as KCNE1 and KCNE3, which are known to shift hELK2 $V_{0.5}$ to more negative V_m [36]. This issue is further discussed in Section 4.2.

In conclusion, in agreement with transcriptomics and protein quantification, mixed hERG1 and hELK2 whole-cell currents were observed in lymphoma cell lines. The corresponding current amplitudes were much smaller in the controls, supporting the notion that EAG-family channels tend to increase their functional expression in cancer cells, and partially substitute $K_{Ca}3.1$ and $K_V1.3$, the main players in normal lymphocytes. We next asked which signaling roles hERG1 and hELK2 exert in lymphoma cells, by first testing whether these K^+ channels participate in macromolecular membrane complexes involving integrin subunits, as was previously observed in other tumors.

3.3. hERG1 (but not hELK2) forms a macromolecular complex with β1 integrin subunits, in lymphoma cells

Considering that the hERG1 contribution to a cancer cell physiology is generally thought to include non-conductive signaling functions [37], we investigated the downstream hERG1-dependent signaling pathways in lymphomas. As discussed earlier, in human tumors, and particularly in aggressive carcinomas, hERG1 is frequently bound to the β1 subunit of integrin receptors, which promotes cancer growth and invasiveness [23]. We thus tested the presence and amount of hERG1-β1 integrin complex in our DLBCL cell lines. To control the timing of β1 integrin expression and complex formation, cells were maintained in serum-free media overnight and seeded on a fibronectin-coated plate for 90 min, before testing. Co-IP experiments were performed by immunoprecipitating proteins with the anti β1 integrin antibody as in [26] and revealing the blot with the anti hERG1 polyclonal antibody. The hERG1/β1 integrin macromolecular complex turned out to be formed in all DLBCL lines, but not in EBV-infected normal lymphocytes (Fig. 3A and the densitometric analysis in Fig. 3B). In the same Co-IPs, the immunoblots were exposed to the anti hELK2 antibody, but no signal was detected, hence ruling out the possibility that hELK2 could be recruited in the hERG1-β1 integrin complex or form a macromolecular complex with β1 integrin alone (Fig. 3C and the densitometric analysis in Fig. 3D). IF staining was then performed with a bispecific antibody that specifically recognizes the hERG1/β1 integrin complex (scDb-hERG1-β1). The complex was found in all the lymphoma cell lines, as well as in hERG1-overexpressing HEK cells, as expected, whereas it was virtually absent in EBV-infected lymphocytes and wild type HEK cells (Fig. 3E and the densitometric analysis in Fig. 3F).

Table 1
Resting potential of lymphoma and control cell lines.

Cell Line	V_{REST} (mV)	C_{CAP} (pF)	Number of cells
EBV-infected lymphocytes	−44.2 ± 8.38	8.8 ± 2.3	8
U2932	−46.9 ± 7.75	15.1 ± 2.4	7
SU-DHL−4	−47.2 ± 5.25	10.5 ± 2.1	7
WSU-DLBCL2	−49.3 ± 3.9	9.1 ± 3.3	9

V_{REST} values in a representative sample of cells expressing recognizable EAG-type currents, in the indicated cell lines. C_{CAP}= cell capacitance; V_{REST} = resting membrane potential.

3.4. The effect of modulating the hERG1-β1 integrin complex formation on lymphoma cell proliferation

We next studied the hERG1-β1 integrin complex formation in the presence of different molecules able to block K^+ channels, or target the complex, or both. In distinct experiments, EBV-immortalized lymphocytes, SU-DHL-4, WSU-DLCL2, and U2932 were treated, for 90 min after cell adhesion to fibronectin, with the following molecules. 1) The hERG1 blocker E4031 (30 μM, to counteract the reduction of free concentration caused by plasma protein binding in serum-containing culture medium; [29]). 2) The wide-spectrum K^+ channel blocker Cs^+ (5 mM), to evaluate the overall K^+ channel contribution. 3) The bispecific scDb-hERG1-β1 antibody, which binds to extracellular epitopes of β1 integrin and hERG1. Because the two corresponding paratopes are connected by a 20-aminoacid linker, the antibody can bind to both epitopes only when they are associated in the macromolecular complex. The bispecific antibody was used at 50–100 μg/mL [38,39]. 4) Clarithromycin (80–160 μM; [40]), a macrolide antibiotic that exerts anti-lymphoproliferative effects by i) down-regulating the anti-apoptotic proteins BCL-2 and BCL-XL [41–43], and ii) inhibiting the intracellular signalling pathways triggering autophagic cell death, by blocking hERG1 [40,44]. Because clarithromycin preferentially binds the closed channel conformation [44,45], it can directly target the hERG1-β1 integrin complex (which recruits the closed channel conformation) and moreover prevent hERG1 from associating to the p85 PI3K subunit [40].

In our cell lines, all the above treatments reduced the amount of hERG1-β1 integrin complex compared to the untreated controls (Fig. 4A and the densitometric analysis in Fig. 4B). The effect was nonetheless stronger with the molecules that directly target the complex (scDb-hERG1-β1 and clarithromycin). Hence, we studied whether these latter treatments affected cell proliferation of SU-DHL-4, WSU-DLCL2 and U2932 lymphoma cells, and EBV-infected lymphocytes (Fig. 5A-D). Both scDb-hERG1-β1 (50 μg/mL) and clarithromycin (160 μM) strongly inhibited cell proliferation. The antiproliferative effect of these molecules was absent in EBV-infected lymphocytes (Fig. 5D), in agreement with the observation that these cells express negligible amounts of the hERG1-β1 macromolecular complex (Fig. 3).

In conclusion, scDb-hERG1-β1 and clarithromycin, *i.e.,* the molecules most effective in reducing the hERG1-β1 integrin complex formation, had a strong impact on proliferation, which points to a functional role of the hERG1-β1 integrin complex in lymphoma cell growth.

3.5. Expression of hERG1 and hERG1-β1 integrin complex in DLBCL and MALT lymphoma patients

The presence of the hERG1-β1 integrin complex was further tested in

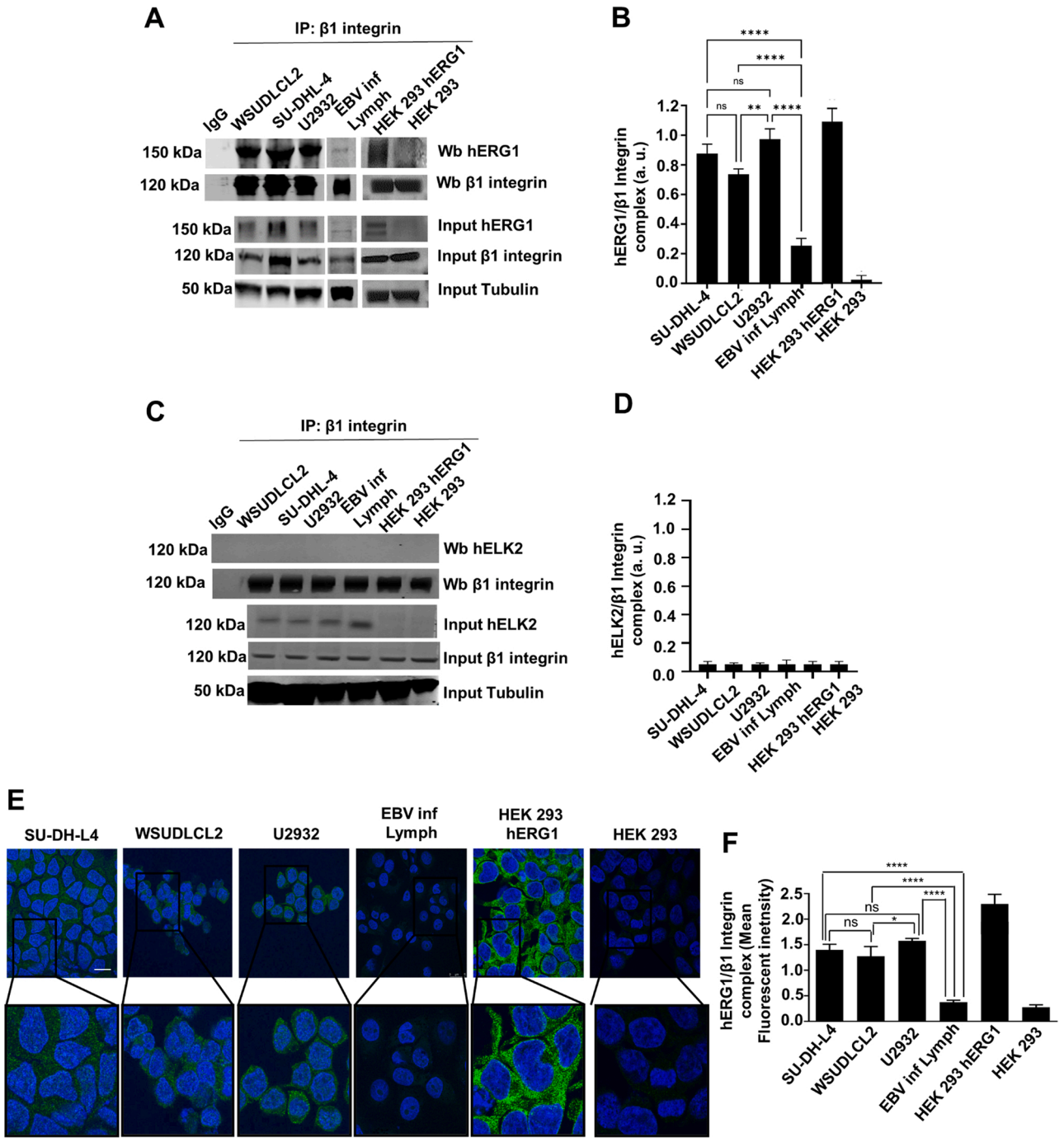

Fig. 3. Expression of the hERG1-β1 integrin complex in DLBCL lymphoma cells. (A) Representative membrane of hERG1/β1 integrin complex in DLBCL lymphoma, HEK 293 and HEK 293 hERG1 cells, seeded on fibronectin for 90 min and immunoprecipitated with anti-β1 integrin (TS2/16). (B) Bar graph reporting the average densitometric results, relative to three different experiments carried out as in (A); a.u. = arbitrary units. Statistical analysis was carried out with one-way ANOVA. (C) Representative membrane of hELK2/β1 integrin complex in DLBCL lymphoma, HEK 293 and HEK 293 hERG1 cells, seeded on fibronectin for 90 min and immunoprecipitated with anti-β1 integrin (TS2/16). (D) Bar graph reporting the average densitometric results, relative to three different experiments carried out as in (C); a.u. = arbitrary units. (E) Representative IF images (scale bar: 100 μm) of the different DLBCL lymphoma, HEK 293 and HEK 293 hERG1 cells, seeded on fibronectin for 90 min and stained with scDb–hERG1–β1. (F) Bar graph reporting the average IF intensity, relative to three different experiments carried out as in (E). For each condition, the fluorescence relative to 20 cells was analyzed. HEK293 and HEK293 hERG1 were used as negative and positive controls. Statistical analysis was carried out with one-way ANOVA.

a cohort of DLBCL patients by using the scDb-hERG1-β1 antibody as a probe. Among the 92 primary DLBCL samples, 22 were negative (0 % of marked cells), while in 70, corresponding to 76 % of all DLBCL, the complex was detected with varying intensity (≥1 % of marked cells). Examples of a negative and a strongly positive sample are shown in Fig. 6A. A statistically significant association with male sex ($p = 0.04$) and a trend close to the statistical significance ($p = 0.07$) with BCL2 expression emerged (Fig. 6B). No survival data were available for these clinical specimens.

Finally, hERG1 expression and the formation of the hERG1-β1 integrin complex were evaluated by immunohistochemistry in a cohort of twenty MALT lymphoma patients treated with clarithromycin (500 or

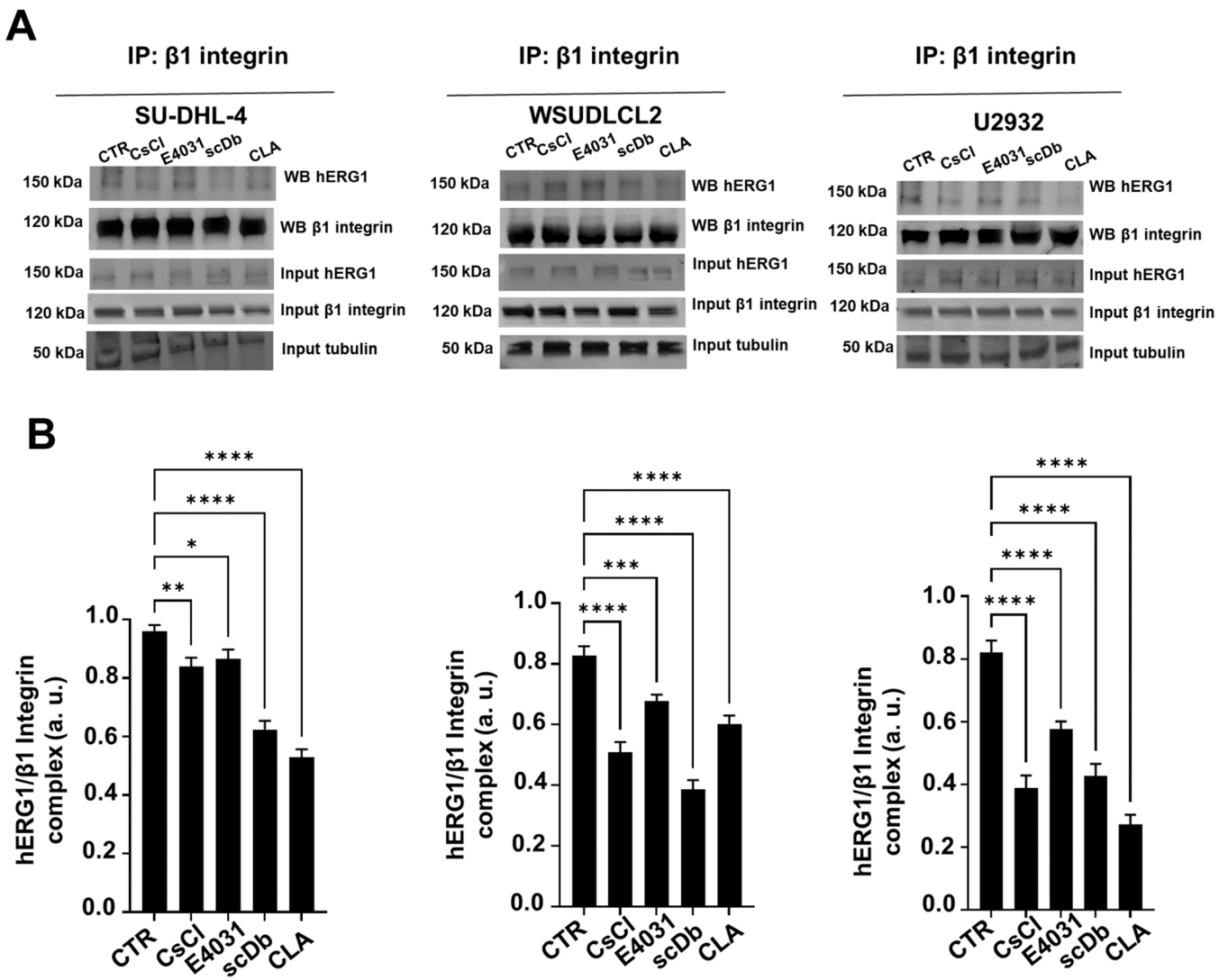

Fig. 4. Effects of different treatment on the hERG1-β1 integrin complex in DLBCL lymphoma cells. (A) Representative blot of hERG1/β1 integrin complex in DLBCL lymphoma cells, seeded on fibronectin for 90 min and treated with CsCl (5 mM), E4031 (30 μM), scDb-hERG1-β1 (100 μg/mL), or clarithromycin (160 μM). Immunoprecipitation was performed with anti-β1 integrin (TS2/16). (B) Bar graph reporting the quantification of the hERG1/β1 integrin complex (determined as detailed in the Materials and Methods) relative to experiments carried out as in (A). Data are presented as mean values ± s.e.m. (n = 3). Statistical analysis was performed by one-way ANOVA. CTR: Control; scDb: scDb-hERG1-β1; CLA: Clarithromycin.

1000 mg, twice a day, administered orally) [46]. The clinical characteristics of the patients are reported in Supplementary Table 3**.** These samples expressed hERG1 (16/20) and the hERG1-β1 integrin complex (11/20) (representative negative and positive samples for the hERG1-β1 integrin complex are shown in Fig. 6C) and showed a 55 % overall response rate to the drug. Notably, in this cohort, a tendency to a higher overall survival probability, despite not being statistically significant, was associated with clarithromycin-treated patients positive for the hERG1-β1 integrin complex (Fig. 6D).

4. Discussion

4.1. K^+ channels in lymphoma cell lines

We studied the expression and function of K^+ channels in 47 human lymphoma cell lines. Among these, a differential expression pattern emerged for *KCNH2, KCNH3, KCNA3* and *KCNN4.* In particular, *KCNH2* and *KCNH3* were detected prevalently in DLBCL and MCL, while *KCNN4* was expressed in all the different lymphoma cell subtypes. In the DLBCL lines SU-DHL-4, WSU-DLCL2 (GCB), and U2932 (ABC), a general reduction of *KCNA3* and *KCNN4* expression was observed, paralleled by a lower membrane amount of the corresponding $K_{Ca}3.1$ and $K_V1.3$, compared to the controls (EBV-infected, and hence immortalized, B lymphocytes). The transcriptomic and biochemical results were in overall agreement with previous electrophysiological data of ours, indicating scarce functional expression of $K_V1.3$ and $K_{Ca}3.1$ in DLBCL lines (with the partial exception of $K_V1.3$ in SU-DHL-4; [33]). Nonetheless, the level of $K_{Ca}3.1$ protein turned out to be comparatively high in SU-DHL-4. This issue was not further investigated. Presumably, a background amount of $K_{Ca}3.1$ protein in our lymphoma cells resided in the endoplasmic reticulum membranes, as this channel is known to present a short half-life at the cell surface, in a variety of cell lines [47]. Moreover, $K_{Ca}3.1$ is also expressed in the inner mitochondrial membrane [48]. Hence, different $K_{Ca}3.1$ protein amounts in the intracellular compartments of distinct lymphoma cell lines could be related to the cell-specific balance of oxidative and glycolytic metabolism.

$K_{Ca}3.1$ and $K_V1.3$ are the main drivers of Ca^{2+} influx during B lymphocyte development and activation [2]. The present observations are consistent with previous results obtained on FLs, suggesting that downregulation of these channel types, accompanied by reduced Ca^{2+}

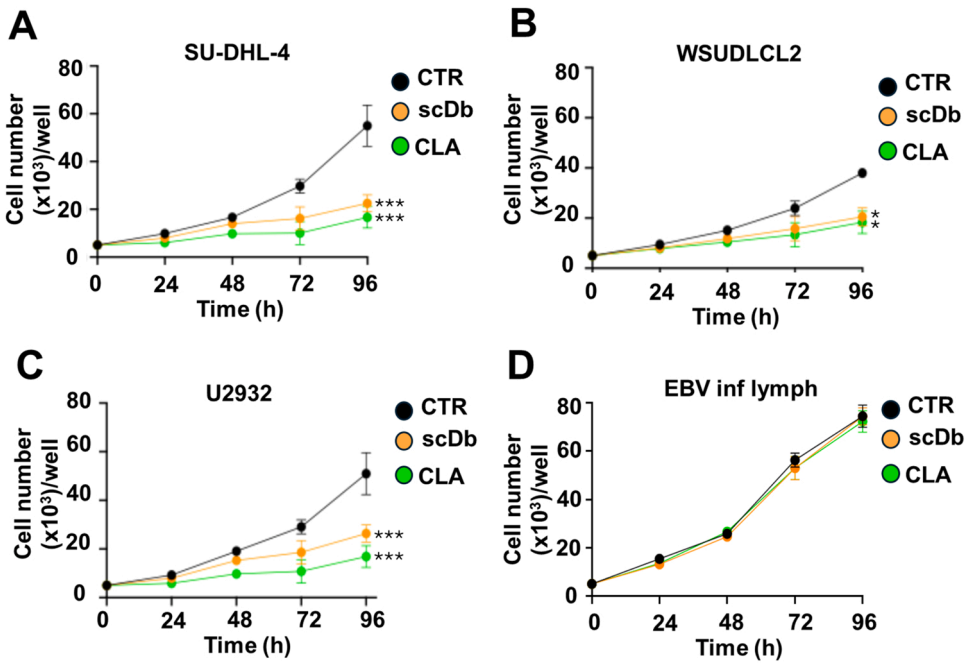

Fig. 5. Effects of different treatments on cell growth of DLBCL lymphoma cells. Curves representing the mean counts of live cells after 24 h, 48 h, 72 h, and 96 h of treatment with scDb-hERG1-β1 (50 μg/mL) and clarithromycin (160 μM) in (A) SU-DHL-4, (B) WSU-DLCL2, (C) U2932 and (D) EBV-infected B lymphocytes. CTR: Control; scDb: scDb-hERG1-β1; CLA: Clarithromycin; EBV inf lymph: EBV-infected B lymphocytes. Statistical analysis was carried out with one-way ANOVA.

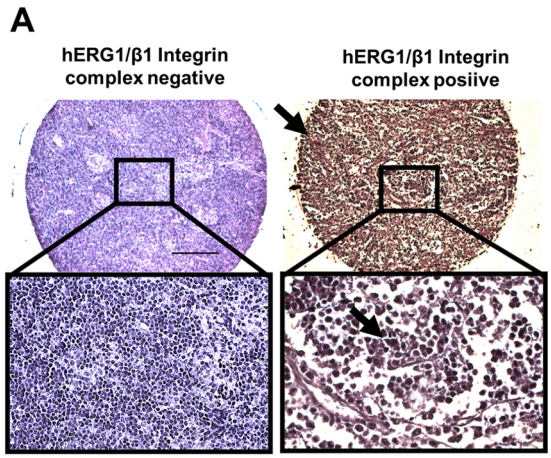

B

Parameter		hERG1/β1 integrin negative	hERG1/β1 integrin positive	P Value
Gender	Female	12 (13%)	21 (23%)	0.04
	Male	10 (11%)	49 (53%)	
Mean Age	<46	13 (14%)	39 (42%)	0.81
	≥46	9 (10%)	31 (34%)	
BCL2	-	2 (2%)	13 (14%)	
	+	3 (3%)	12 (13%)	0.07
	++	2 (2%)	19 (21%)	
	+++	15 (16%)	25 (27%)	
CD20	-	1 (1%)	11 (12%)	
	+	1 (1%)	5 (5%)	0.63
	++	8 (9%)	21 (23%)	
	+++	12 (13%)	33 (36%)	

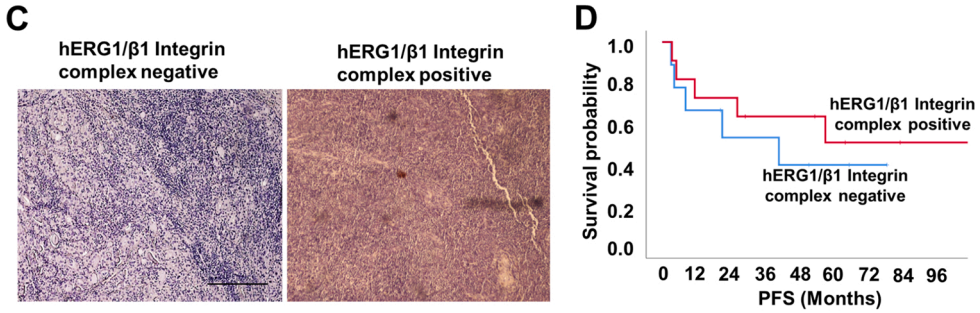

Fig. 6. Expression and clinical relevance of the hERG1/β1 integrin complex in primary lymphoma samples. (A) Representative IHC images of hERG1/β1 integrin complex expression in DLBCL samples. The staining was performed with scDb-hERG1-β1 as reported in Section 2.10. Left panel: hERG1/β1 integrin complex negative sample; right panel: hERG1/β1 integrin complex positive sample (scale bar: 100 μm). (B) Table reporting the number and percentage of negative and positive samples, and the associations between hERG1/β1 integrin complex expression and clinicopathological characteristics of DLBCL samples. (C) Representative IHC images of hERG1/β1 integrin complex expression in primary MALT lymphoma samples. The staining was performed with scDb-hERG1-β1 as reported in Section 2.10. Left panel: hERG1/β1 integrin complex negative sample; right panel: hERG1/β1 integrin complex positive sample (scale bar: 100 μm). (D) Kaplan Meier curves of progression-free survival obtained from the risk analysis of 20 MALT lymphoma patients treated with clarithromycin. In red, patients positive for hERG1/β1 integrin complex (11/20); blue, negative patients (9/20). Statistical analysis was performed using the Long-rank test.

signaling in response to antigen stimulation, accompany DLBCL lymphoma onset and progression [13]. Such alteration of the K^+ channel complement in lymphoma cell lines appears thus to be associated with a modified Ca^{2+} homeostasis during the neoplastic transformation. Notably, $K_V1.3$ dysregulation or block can alter the immune response, relieve radiation-induced neurotoxic effects or affect cancer growth [49,50], whereas $K_{Ca}3.1$ is mainly deregulated during tumor progression, which contributes to malignancy [51].

In all DLBCL lines, downregulation of $K_{Ca}3.1$ and $K_V1.3$ was accompanied by increased expression of *KCNH2* and *KCNH3* transcripts and proteins. Patch-clamp measurements revealed hERG1 currents in SU-DHL-4, WSU-DLCL2 and U2932 cells, and particularly an increased E4031-sensitive current, compared to EBV-immortalized lymphocytes, which are characterized by a low *KCNH2* expression. Functional expression of hERG1 in these cells is consistent with recent studies showing that aberrant selection of B cell precursors is associated to hERG1 blockage [52]. Up-regulation of hERG1 has been previously evidenced in B-cells and associated with the onset of B-cell leukemia [16,17], thus suggesting its implication in lymphoma malignant transformation. In addition, lymphoma cell lines presented voltage-gated K^+ channels with biophysical features similar to the hERG1's, which were insensitive to the known hERG1 blockers, but responsive to Cs^+ [28]. Considering the transcriptomic data, the best candidate is hELK2, as *KCNH3* was expressed in all DLBCL lines. Moreover, the voltage-dependence and kinetics of the E4031-insensitive currents are consistent with the typical properties of hELK2 currents [28]. Evidence is slowly emerging about the implication of *KCNH3* in tumors. Recent genomic results correlate *KCNH3* variants with prostate cancer malignancy [31], and *KCNH3* has been implicated in ovarian cancer progression [30] and included in a risk score system for clear cell renal cell carcinoma [53]. The observation of hELK2 currents in tumors outside the nervous system, and particularly in lymphomas, is novel. At the present stage, the specific functional role of hELK2 channels in cancer progression and its interplay with hERG1 remain uncertain. Our results suggest that hERG1 and hELK2 are interchangeable as regulators of V_{REST}, thus offering lymphoma cells considerable flexibility in modulating V_m, even after $K_V1.3$ and $K_{Ca}3.1$ downregulation. On the other side, the involvement of hERG1 and hELK2 in intracellular signaling, and the consequent contribution to neoplastic cell proliferation, appear to be distinct, as discussed in the next section.

4.2. The hERG1-β1 integrin complex in lymphoma cell lines and its role in regulating cell proliferation

As a first step to understand the biological role of the two EAG family channels, we investigated the implication of hERG1 in the formation of a macromolecular complex with the β1 integrin subunit, which has been demonstrated in several tumor cells and primary clinical tumor samples, as reviewed in [23]. The hERG1-β1 integrin complex was detected in all the DLBCL cell lines, but scarcely in EBV-immortalized lymphocytes. Notably, hELK2 did not display appreciable co-immunoprecipitation with β1 integrin, which argues against the formation of an hELK2-β1 integrin complex in lymphoma cells. Thus, despite its biophysical and structural similarity with hERG1, hELK2 does not physically associate with β1 integrins, regardless of the hERG1/hELK2 expression ratio. Whether this is caused by a stronger competition for hELK2 binding of the accessory subunits KCNE1 or KCNE3, which tends to exclude the channel association with β1 integrin [26], remains to be determined. A stronger association of hELK2 with the classic accessory subunits would also explain a more negative $V_{0.5}$ of the activation curve [36].

To study the specific role of the hERG1-β1 integrin complex in DLBCL cells, we first assessed different treatments that impair the macromolecular complex formation. The stronger effect was exerted by the two molecules that directly target the complex components (i.e., scDb-hERG1-β1 [38] and clarithromycin [40]). Nonetheless, Cs^+ and E4031 also impaired the hERG1-β1 integrin complex formation. We attribute the latter effect to the open channel block produced by these inhibitors, which sustains the open conformational state of hERG1 that hampers channel association with β1 integrin [26].

We next demonstrated that the molecules that consistently disrupt the hERG1-β1 integrin complex strongly decrease the proliferation of DLBCL lines, with little effect on EBV-infected B lymphocytes, which is consistent with the low amount of the macromolecular complex in the latter cells. Notably, clarithromycin is also known to prevent the association of hERG1 and the PI3K p85 subunit [40]. Whether the same applies to scDb-hERG1-β1 is still unknown. Regardless of the mechanistic details, our results provide a possible unifying picture of the action of these drugs on tumors. In particular, scDb-hERG1-β1 was found to impair cancer cell motility, angiogenesis, and metastasis in preclinical studies on solid tumors, while clarithromycin presents anti-lymphoproliferative activity and has been reported by several clinical reports to be effective in the treatment of different malignant lymphomas and plasma cell disorders [41–43,46].

4.3. The hERG1-β1 integrin complex in clinical lymphoma samples

Expression of the hERG1-β1 integrin complex was also evaluated in primary DLBCL samples by immunohistochemistry. A plasma membrane and cytoplasmic positivity was detected in 76 % of all DLBCL, although to different extents. Although a significant association with male sex was observed, a limitation to the generalisability of the present study is that it did not further consider gender/sex issues. Nonetheless, our results suggest that the hERG1 interplay with integrin receptors is also operant *in vivo*, in agreement with previous observations in human samples (reviewed in [23]), and are consistent with the observation that $K_{Ca}3.1$ is generally downregulated in DLBCL cell lines. Such reorganization of the K^+ channel complement in lymphomas could promote proliferative and metastasizing phenotypes in more aggressive lymphoma clones, possibly associated with a reduced Ca^{2+} response on antigen stimulation during lymphoma progression, as previously hypothesized [54]. A tight coordination of $K_{Ca}3.1$ and hERG1 expression and function appears to be particularly relevant for tumor progression, as is also suggested by previous results in colorectal cancer cells, where expression of the two channel types is reciprocally regulated [55]. What is more, the combination of $K_{Ca}3.1$ activators and hERG1 blockers exerts synergic effects with cisplatin in inhibiting proliferation and stimulating apoptosis [55].

Clinical specimens of MALT lymphoma patients also presented the hERG1-β1 integrin complex and were found to be especially sensitive to the effect of clarithromycin. Data recorded in the limited sample of MALT lymphoma patients suggest a tendency for increased survival probability in the clarithromycin-treated patients positive for the hERG1-β1 integrin complex. Unfortunately, the lack of survival data for our DLBCL clinical specimens prevents a full clarification of the hERG1-β1 integrin role in tumor malignancy. Nonetheless, clarithromycin has been tested for the treatment of various malignant lymphomas and plasma cell disorders in numerous studies and clinical reports [41–43,46]. In particular, in the clinical study whose data are shown in Fig. 4 [46] clarithromycin was administered at doses (500 or 1000 mg) which lead to plasma concentrations of approximately 2–3 μg/mL [56–58], and values 5–10 times as high in interstitial fluids and up to ~600 μg/mL in cells such as alveolar macrophages [57,58]. These concentrations are compatible with those used in our *in vitro* assay and with the range of concentrations effective on hERG1 (IC_{50} of ~30–50 μM; [45]).

The mechanism by which clarithromycin inhibits lymphoproliferative disorders has been hypothesized to be related to its effects on BCL-2 and BCL-xL [41], based on *in vitro* data in murine lymphoma cells obtained with doses of 3.2 μg/mL [42]. However, clarithromycin can also downregulate the intracellular signaling pathways centered on ERK 1/2 and Akt in human myeloid and lymphoid leukemia cells [44], when tested *in vitro* at 36–56 μM (~30−40 μg/mL). It is also worth noting that the action of macrolide antibiotics on hERG1 is complex and may involve intracellular binding sites [59]. Considering that in our

lymphoma cell lines the effect of clarithromycin paralleled the one exerted by scDb-hERG1-β1, we conclude that impairment of hERG1 interaction with β1 integrin and PI3K [37,40] is a major determinant of the antibiotic efficacy.

4.4. Conclusions

We found the K^+ channel profile in DLBCL lymphoma cell lines to be considerably altered compared to non-neoplastic B-lymphocytes, with a tendency for $K_V1.3$ and $K_{Ca}3.1$ to be replaced by the EAG family channels hERG1 and hELK2. These channel types present analogous voltage-dependent properties, which could sustain the different V_m modulation requirements of cancer cells. And yet, major differences emerged in how hERG1 and hELK2 contribute to intracellular signaling mechanisms. On cell adhesion to the extracellular matrix, hERG1, but not hELK2, associated with β1 integrins to form macromolecular membrane complexes in all DLBCL lines. This suggests hERG1 is involved in the downstream signaling pathway centred on Akt and HIF-1a, which sustains the rapid growth rate of DLBCL cells. Disrupting the hERG1-β1 integrin complex with the bispecific scDb-hERG1-β1, or clarithromycin, impaired lymphoma cell proliferation. These effects are consistent with previous observations which could explain the apoptosis and cell cycle modulatory effects of the bispecific antibody [38].

Besides better elucidating the complex interplay between K^+ channels, adhesion receptors, and tumor aggression, the present results in lymphoma cell lines and clinical samples support the notion that the hERG1-β1 integrin complex could serve as a new therapeutic target in DLBCL. Importantly, such a complex is not found in cardiac cells, where hERG1 associates with the accessory subunit KCNE1 [23,26]. Using scDb-hERG1-β1 for cancer therapy would thus avoid the cardiac side effects (i.e., proarrhythmic) exerted by many hERG1 blockers.

Author statement

CS, JI, CD, AA and AB designed and conducted most of the experiments and data analysis. CS, JI, CD. AA and AB wrote the paper. AA and AB supervised the study. FB provided valuable clinical and molecular biology insights. AM and LCG performed and analyzed the electrophysiological recordings. LC and FB performed the RNAseq analysis. MR provided MALT lymphoma samples and performed survival analysis. All authors revised the paper.

CRediT authorship contribution statement

Markus Raderer: Formal analysis. **Luciano Cascione:** Formal analysis. **Annarosa Arcangeli:** Writing – original draft, Supervision, Resources, Project administration, Funding acquisition, Conceptualization. **Francesco Bertoni:** Supervision, Formal analysis. **Andrea Becchetti:** Writing – original draft, Supervision, Project administration, Funding acquisition, Data curation, Conceptualization. **Cesare Sala:** Writing – original draft, Methodology, Investigation, Formal analysis, Data curation, Conceptualization. **Claudia Duranti:** Writing – original draft, Validation, Formal analysis, Data curation. **Jessica Iorio:** Writing – original draft, Methodology, Investigation, Formal analysis, Data curation. **Laura Clara Grandi:** Writing – original draft, Formal analysis, Data curation. **Alberto Montalbano:** Writing – original draft, Methodology, Investigation, Formal analysis, Data curation.

Declaration of Competing Interest

The authors declare that they have no known competing financial interests or personal relationships that could have appeared to influence the work reported in this paper.

Acknowledgments

This work was supported by Associazione Italiana per la Ricerca sul Cancro (grant numbers 21510 and 30874 to A. A.), the University of Milano-Bicocca (2023-ATE-0093 and 2024-ATE-0117 to A. Becchetti), and the University of Florence (ex 60 % to A. A.), and The European Union–NextGenerationEU - National Recovery and Resilience Plan, Mission 4 Component 2 - Investment 1.5 - Tuscany Health Ecosystem - ECS00000017 - CUP B83C22003920001 to A. A.

We thank Dr. Ginevra Chioccioli Altadonna (Department of Experimental and Clinical Medicine, University of Florence, Italy), Dr. Afua Adjeiwaa Mensah and Dr. Alberto Jesus Arribas (Institute of Oncology Research, Faculty of Biomedical Sciences, USI, Bellinzona, Switzerland) for doing some preliminary experiments. Thanks are also due to Dr. Matteo Lulli (Department of Experimental and Clinical Biomedical Sciences, University of Florence) for assistance in IF images acquisition.

Direct URL to data

$K_V1.3$: DHL-4: https://zenodo.org/record/4289852#.X843PulKho4
WSUDLCL2: https://zenodo.org/record/4289856#.X84xrelKho4
EBV lymphocytes: https://zenodo.org/record/4289858#.X8428ulKho4
KCa3.1: DHL-4: https://zenodo.org/record/4289859#.X84 × 4-lKho4
WSUDLCL2: https://zenodo.org/record/4289872#.X84yL-lKho4
EBV-infected lymphocytes: https://zenodo.org/record/4289870#.X84yfulKho4

Appendix A. Supporting information

Supplementary data associated with this article can be found in the online version at doi:10.1016/j.phrs.2025.107992.

Data availability

Details and data relative to $K_V1.3$ and $K_{Ca}3.1$ current recording are available in the Zenodo repository.

References

[1] S. Feske, E.Y. Skolnik, M. Prakriya, Ion channels and transporters in lymphocyte function and immunity, Nat. Rev. Immunol. 12 (2012), https://doi.org/10.1038/nri3233.
[2] K.G. Chandy, H. Wulff, C. Beeton, M. Pennington, G.A. Gutman, M.D. Cahalan, K+ channels as targets for specific immunomodulation, Trends Pharmacol. Sci. 25 (2004) 280–289, https://doi.org/10.1016/j.tips.2004.03.010.
[3] M.D. Cahalan, K.G. Chandy, The functional network of ion channels in t lymphocytes, Immunol. Rev. 231 (2009) 59–87, https://doi.org/10.1111/j.1600-065X.2009.00816.x.
[4] R.S. Lewis, M.D. Cahalan, Potassium and calcium channels in lymphocytes, Annu. Rev. Immunol. 13 (1995) 623–653, https://doi.org/10.1146/annurev.iy.13.040195.003203.
[5] M.D. Cahalan, K.G. Chandy, T.E. DeCoursey, S. Gupta, A voltage-gated potassium channel in human t lymphocytes, J. Physiol. 358 (1985) 197–237, https://doi.org/10.1113/jphysiol.1985.sp015548.
[6] F. Bezanilla, How membrane proteins sense voltage, Nat. Rev. Mol. Cell. Biol. 9 (2008) 323–332, https://doi.org/10.1038/nrm2376.
[7] X.M. Xia, B. Fakler, A. Rivard, G. Wayman, T. Johnson-Pais, J.E. Keen, T. Ishii, B. Hirschberg, C.T. Bond, S. Lutsenko, J. Maylie, J.P. Adelman, Mechanism of calcium gating in small-conductance calcium-activated potassium channels, Nat 395 (1998) 503–507, https://doi.org/10.1038/26758.
[8] Y. Wang, A. Tao, M. Vaeth, S. Feske, Calcium regulation of t cell metabolism, Curr. Opin. Physiol. 17 (2020) 207–223, https://doi.org/10.1016/j.cophys.2020.07.016.
[9] C. Beeton, H. Wulff, J. Barbaria, O. Clot-Faybesse, M. Pennington, D. Bernard, M. D. Cahalan, K.G. Chandy, E. Béraud, Selective blockade of t lymphocyte K(+) channels ameliorates experimental autoimmune encephalomyelitis, a model for multiple sclerosis, Proc. Natl. Acad. Sci. USA 98 (2001) 13942–13947, https://doi.org/10.1073/pnas.241497298.
[10] R.J. Leonard, M.L. Garcia, R.S. Slaughter, J.P. Reuben, Selective blockers of voltage-gated K^+ channels depolarize human t lymphocytes: mechanism of the antiproliferative effect of charybdotoxin, Proc. Natl. Acad. Sci. USA 89 (1992) 10094–10098, https://doi.org/10.1073/pnas.89.21.10094.

[11] S. Srivastava, K. Ko, P. Choudhury, Z. Li, A.K. Johnson, V. Nadkarni, D. Unutmaz, W.A. Coetzee, E.Y. Skolnik, Phosphatidylinositol-3 phosphatase myotubularin-related protein 6 negatively regulates CD4 t cells, Mol. Cell Biol. 26 (2006) 5595–5602, https://doi.org/10.1128/MCB.00352-06.

[12] A. Arcangeli, S. Pillozzi, A. Becchetti, Targeting ion channels in leukemias: a new challenge for treatment, Curr. Med Chem. 19 (2012) 683–696, https://doi.org/10.2174/092986712798992093.

[13] E. Lastraioli, J. Iorio, A. Arcangeli, Ion channel expression as promising cancer biomarker, Biochim. Biophys. Acta 1848 (2015) 2685–2702, https://doi.org/10.1016/j.bbamem.2014.12.016.

[14] A. Magi, M. Masselli, C. Sala, A. Guerriero, P. Laise, B. Puccini, L. Rigacci, C. Breschi, O. Crociani, S. Pillozzi, A. Arcangeli, The ion channels and transporters gene expression profile indicates a shift in excitability and metabolisms during malignant progression of follicular lymphoma, Sci. Rep. 9 (2019) 8586, https://doi.org/10.1038/s41598-019-44661-x.

[15] G.A.M. Smith, H.W. Tsui, E.W. Newell, X. Jiang X, X.P. Zhu, F.W.L. Tsui, L. C. Schlichter LC, Functional up-regulation of HERG K+ channels in neoplastic hematopoietic cells, J. Biol. Chem. 277 (2002) 18528–18534, https://doi.org/10.1074/jbc.M200592200.

[16] S. Pillozzi, A. Accordi, P. Rebora, V. Serafin, M.G. Valsecchi, G. Basso, A. Arcangeli, Differential expression of hERG1A and hERG1B genes in pediatric acute lymphoblastic leukemia identifies different prognostic subgroups, Leukemia 28 (2014) 1352–1355, https://doi.org/10.1038/leu.2014.26.

[17] S. Pillozzi, M. Masselli, E. De Lorenzo, B. Accordi, E. Cilia, O. Crociani, A. Amedei, M. Veltroni, M. D'Amico, G. Basso, A. Becchetti, D. Campana, A. Arcangeli, Chemotherapy resistance in acute lymphoblastic leukemia requires hERG1 channels and is overcome by hERG1 blockers, Blood 117 (2011) 902–914, https://doi.org/10.1182/blood-2010-01-262691.

[18] L.M. Morton, S.S. Wang, S.S. Devesa, P. Hartge, D.D. Weisenburger, M.S. Linet, Lymphoma incidence patterns by WHO subtype in the United States, 1992-2001, Blood 107 (2006) 265–276, https://doi.org/10.1182/blood-2005-06-2508.

[19] S. Novelli, J. Briones, J. Sierra, Epidemiology of lymphoid malignancies: last decade update, SpringerPlus 2 (2013) 70, https://doi.org/10.1186/2193-1801-2-70.

[20] J.M. Irish, J.H. Myklebust, A.A. Alizadeh, R. Houot, J.P. Sharman, D.K. Czerwinski, G.P. Nolan, R. Levy, B-cell signaling networks reveal a negative prognostic human lymphoma cell subset that emerges during tumor progression, Proc. Natl. Acad. Sci. USA 107 (2010) 12747–12754, https://doi.org/10.1073/pnas.1002057107.

[21] N.A. Castle, Pharmacological modulation of voltage-gated potassium channels as a therapeutic strategy, Expert Opin. Ther. Pat. 20 (2010) 1471–1503, https://doi.org/10.1517/13543776.2010.513384.

[22] L. Bianchi, B. Wible, A. Arcangeli, M. Taglialatela, F. Morra, P. Castaldo, O. Crociani, B. Rosati, L. Faravelli, M. Olivotto, E. Wanke, *herg* encodes a K^+ current highly conserved in tumors of different histogenesis: a selective advantage for cancer cells? Cancer Res 58 (1998) 815–822.

[23] A. Arcangeli, J. Iorio, C. Duranti, Targeting the hERG1 and β1 integrin complex for cancer treatment, Expert Opin. Ther. Targets 28 (2024) 145–157, https://doi.org/10.1080/14728222.2024.2318449.

[24] S. Pillozzi, M.F. Brizzi, M. Balzi, O. Crociani, A. Cherubini, L. Guasti, B. Bartolozzi, A. Becchetti, E. Wanke, P.A. Bernabei, M. Olivotto, L. Pegoraro, A. Arcangeli, HERG potassium channels are constitutively expressed in primary human acute myeloid leukemias and regulate cell proliferation of normal and leukemic hemopoietic progenitors, Leukemia 16 (2002) 1791–1798, https://doi.org/10.1038/sj.leu.2402572.

[25] S. Pillozzi, M.F. Brizzi, P.A. Bernabei, B. Bartolozzi, R. Caporale, V. Basile, V. Boddi V, L. Pegoraro, A. Becchetti, A. Arcangeli, VEGFR-1 (FLT-1), beta1 integrin, and hERG K+ channel for a macromolecular signaling complex in acute myeloid leukemia: role in cell migration and clinical outcome, Blood 110 (2007) 1238–1250, https://doi.org/10.1182/blood-2006-02-003772.

[26] A. Becchetti, S. Crescioli, F. Zanieri, G. Petroni, R. Mercatelli, S. Coppola, L. Gasparoli, M. D'Amico, S. Pillozzi, O. Crociani, M. Stefanini, A. Fiore, L. Carraresi, V. Morello, S. Manoli, M.F. Brizzi, D. Ricci, M. Rinaldi, A. Masi, T. Schmidt, F. Quercioli, P. Defilippi, A. Arcangeli, The conformational state of hERG1 channels determines integrin association, downstream signaling, and cancer progression, Sci. Signal 10 (2017) eaaf3236, https://doi.org/10.1126/scisignal.aaf3236.

[27] A. Becchetti, C. Duranti, A. Arcangeli, Dynamics and physiological meaning of complexes between ion channels and integrin receptors: the case of Kv11.1, Am. J. Physiol. Cell. Physiol. 322 (2022) C1138–C1150, https://doi.org/10.1152/ajpcell.00107.2022.

[28] A. Becchetti, M. De Fusco, O. Crociani, A. Cherubini, R. Restano-Cassulini, M. Lecchi, A. Masi, A. Arcangeli, G. Casari, E. Wanke, The functional properties of the human *ether-à-go-go*-like (HELK2) K^+ channel, Eur. J. Neurosci. 16 (2002) 415–428, https://doi.org/10.1046/j.1460-9568.2002.02079.x.

[29] A. Masi, A. Becchetti, R. Restano-Cassulini, S. Polvani, G. Hofmann, A. M. Buccoliero, M. Paglierani, B. Pollo, G.L. Taddei, P. Gallina, N. Di Lorenzo, S. Franceschetti, E. Wanke, A. Arcangeli, hERG1 channels are overexpressed in glioblastoma multiforme and modulate VEGF secretion in glioblastoma cell lines, Br. J. Cancer 93 (2005) 781–792, https://doi.org/10.1038/sj.bjc.6602775.

[30] Z. Li, L. Huang, L. Wei, B. Zhang, S. Zhong, Y. Ou, C. Wen, S. Huang, KCNH3 predicts poor prognosis and promotes progression in ovarian cancer, Onco. Targets Ther. 13 (2020) 10323–10333, https://doi.org/10.2147/OTT.S268055.

[31] S. Weiss, P. Lamy, M. Rusan, M. Nørgaard, B.P. Ulhøi, M. Knudsen, C.G. Kassentoft, L. Farajzadeh, J.B. Jensen, J.S. Pedersen, M. Borre, K.D. Sørensen, Exploring the tumor genomic landscape of aggressive prostate cancer by whole-genome sequencing of tissue or liquid biopsies, Int. J. Cancer 155 (2024) 298–313, https://doi.org/10.1002/ijc.34949.

[32] Z. Johnson, C. Tarantelli, E. Civanelli, L. Cascione, F. Spriano, A. Fraser, P. Shah, T. Nomanbhoy, S. Napoli, A. Rinaldi, K. Niewola-Staszkowska, M. Lahn, D. Perrin, M. Wenes, D. Migliorini, F. Bertoni, L. van der Veen, G. Di Conza, IOA-244 is a non-ATP-competitive, highly selective, tolerable PI3K delta inhibitor that targets solid tumors and breaks immune tolerance, Cancer Res Commun. 3 (2023) 576–591, https://doi.org/10.1158/2767-9764.CRC-22-0477.

[33] A. Montalbano, C. Sala, G.C. Altadonna, A. Becchetti, A. Arcangeli, High throughput clone screening on overexpressed hERG1 and Kv1.3 potassium channels using ion channel reader (ICR) label free technology, Heliyon 9 (2023) e20112, https://doi.org/10.1016/j.heliyon.2023.e20112.

[34] A. Montalbano, C. Sala, C. Abrardo, N. Murciano, F. Jahanfar, M. D'Amico, F. Bertoni, A. Becchetti, A. Arcangeli, Data describing the effects of potassium channels modulators on outward currents measured in human lymphoma cell lines, Data Brief. 34 (2021) 106668, https://doi.org/10.1016/j.dib.2020.106668.

[35] R. Schönherr, B. Rosati, S. Hehl, V.G. Rao, A. Arcangeli, M. Olivotto, S. H. Heinemann, E. Wanke, Functional role of the slow activation property of ERG K^+ channels, Eur. J. Neurosci. 11 (1999) 753–760, https://doi.org/10.1046/j.1460-9568.1999.00493.x.

[36] S.M. Clancy, B. Chen, F. Bertaso, J. Mamet, T. Jegla, KCNE1 and KCNE3 β-subunits regulate membrane surface expression of Kv12.2 K^+ channels *in vitro* and form a tripartite complex *in vivo*, PLoS ONE 4 (2009) e6330, https://doi.org/10.1371/journal.pone.0006330.

[37] A. Becchetti, G. Petroni, A. Arcangeli, Ion channel conformations regulate integrin-dependent signaling, Trends Cell. Biol. 29 (2019) 298–307, https://doi.org/10.1016/j.tcb.2018.12.005.

[38] C. Duranti, J. Iorio, G. Bagni, G. Chioccioli Altadonna, T. Fillion, M. Lulli, F. N. D'Alessandro, A. Montalbano, E. Lastraioli, D. Fanelli, S. Coppola, T. Schmidt, F. Piazza, A. Becchetti, A. Arcangeli, Integrins regulate hERG1 dynamics by girdin-dependent Gαi3: signaling and modeling in cancer cells, Life Sci. Alliance 7 (2024) e202302135, https://doi.org/10.26508/lsa.202302135.

[39] C. Duranti, J. Iorio, T. Lottini, E. Lastraioli, S. Crescioli, G. Bagni, M. Lulli, C. Capitani, R. Bouazzi, M. Stefanini, L. Carraresi, L. Iamele, H. De Jonge, A. Arcangeli, Harnessing the hERG1/β1 integrin complex via a novel bispecific single-chain antibody: an effective strategy against solid cancers, Mol. Cancer Ther. 20 (2021) 1338–1349, https://doi.org/10.1158/1535-7163.MCT-20-1111.

[40] G. Petroni, G. Bagni, J. Iorio, C. Duranti, T. Lottini, M. Stefanini, G. Kragol, A. Becchetti, A. Arcangeli, Clarithromycin inhibits autophagy in colorectal cancer by regulating the hERG1 potassium channel interaction with PI3K, Cell Death Dis. 11 (2020) 161, https://doi.org/10.1038/s41419-020-2349-8.

[41] M. Ohe, S. Hashino, A case of follicular B-cell lymphoma treated using clarithromycin, Korean J. Hematol. 46 (2011) 203, https://doi.org/10.5045/kjh.2011.46.3.203.

[42] T. Ohara, T. Morishita, H. Suzuki, T. Masaoka, H. Ishii, T. Hibi, Antibiotics directly induce apoptosis in b cell lymphoma cells devived from BALB/c mice, Anticancer Res 24 (2004) 3723–3730.

[43] Y. Ishimatsu, H. Mukae, K. Matsumoto, T. Harada, A. Hara, S. Hara, M. Amenomori, H. Fujita, N. Sakamoto, T. Hayashi, S. Kohno, Two cases with pulmonary mucosa-associated lymphoid tissue lymphoma successfully treated with clarithromycin, Chest 138 (2010) 730–733, https://doi.org/10.1378/chest.09-2358.

[44] S. Pillozzi, M. Masselli, L. Gasparoli, M. D'Amico, L. Polletta, M. Veltroni, C. Favre, G. Basso, A. Becchetti, A. Arcangeli, Macrolide antibiotics exert antileukemic effects by modulating the autophagic flux through inhibition of hERG1 potassium channels, Blood Cancer J. 6 (2016) e423, https://doi.org/10.1038/bcj.2016.32.

[45] W.A. Volberg, B.J. Koci, W. Su, J. Lin, J. Zhou, Blockade of human cardiac potassium channel human ether-a-go-go-related gene (HERG) by macrolide antibiotics, J. Pharmacol. Exp. Ther. 302 (2002) 320–327, https://doi.org/10.1124/jpet.302.1.320.

[46] A.J.M. Ferreri, M. Sassone, B. Kiesewetter, S. Govi, L. Scarfò, G. Donadoni, M. Raderer, High-dose clarithromycin is an active monotherapy for patients with relapsed/refractory extranodal marginal zone lymphoma of mucosa-associated lymphoid tissue (MALT): the HD-K phase II trial, Ann. Oncol. 26 (2015) 1760–1765, https://doi.org/10.1093/annonc/mdv214.

[47] C.M. Balut, Y. Gao, S.A. Murray, P.H. Thibodeau, D.C. Devor, ESCRT-dependent targeting of plasma membrane localized KCa3.1 to the lysosomes, Am. J. Physiol. Cell Physiol. 299 (2010) C1015–C1027, https://doi.org/10.1152/ajpcell.00120.2010.

[48] L. Leanza, V. Cecchetto, L. Bisutto, A. Rossa, R. Costa, M. Bachmann, M. Zoratti, I. Szabo, Pharmacological modulation of mitochondrial ion channels, Brit. J. Pharm. 176 (2019) 4258–4283, https://doi.org/10.1111/bph.14544.

[49] N. Comes, J. Bielanska, A. Vallejo-Gracia, A. Serrano-Albarrás, L. Marruecos, D. Gómez, C. Soler, E. Condom, Y. Ramón, S. Cajal, J. Hernández-Losa, J. C. Ferreres, A. Felipe, The voltage-dependent K(+) channels Kv1.3 and Kv1.5 in human cancer, Front. Physiol. 4 (2013) 283, https://doi.org/10.3389/fphys.2013.00283.

[50] Y. Peng, K. Lu, Z. Li, Y. Zhao, Y. Wang, B. Hu, P. Xu, X. Shi, B. Zhou, M. Pennington, K.G. Chandy, Y. Tang, Blockade of Kv1.3 channels ameliorates radiation-induced brain injury, NeuroOncol. 16 (2014) 528–539, https://doi.org/10.1093/neuonc/not221.

[51] L.M. Todesca, S. Maskri, K. Brömmel, I. Thale, B. Wünsch, O. Koch, A. Schwab, Targeting $K_{Ca}3.1$ channels in cancer, Cell Physiol. Biochem 55 (2021) 131–144, https://doi.org/10.33594/000000374.

[52] C. Sala, M. Staderini, T. Lottini, C. Duranti, G. Angelini, G. Constantin, A. Arcangeli, Expression of the ether-a-gò-gò-related gene 1 channel during b and t

lymphocyte development: role in BCR and TCR signaling, Front Immunol. 14 (2023) 1111471, https://doi.org/10.3389/fimmu.2023.1111471.
[53] C. Zhang, F. Wang, F. Guo, C. Ye, Y. Yang, Y. Huang, J. Hou, F. Tian, B. Yang, A 13-gene risk score system and a nomogram survival model for predicting the prognosis of clear cell renal cell carcinoma, Urol. Oncol. 3874 (2019) e1–74.e11, https://doi.org/10.1016/j.urolonc.2019.12.022.
[54] C. Sala, A. Arcangeli, Reduced BCR signaling and a metabolic shift accompanies malignant progression of follicular lymphoma: a lesson from transcriptomics, Arch. Cancer Biol. Ther. 1 (2020), https://doi.org/10.33696/cancerbiology.1.007.
[55] S. Pillozzi, M. D'Amico, G. Bartoli, L. Gasparoli, G. Petroni, O. Crociani, T. Marzo, A. Guerriero, L. Messori, M. Severi, R. Udisti, H. Wulff, K.G. Chandy, A. Becchetti, A. Arcangeli, The combined activation of KCa3.1 and inhibition of Kv11.1/hERG1 currents contribute to overcome cisplatin resistance in colorectal cancer cells, Brit. J. Cancer 118 (2018) 200–212, https://doi.org/10.1038/bjc.2017.392.
[56] M.H. Gotfried, L.H. Danziger, K.A. Rodvold, Steady-state plasma and bronchopulmonary characteristics of clarithromycin extended-release tablets in normal healthy adult subjects, J. Antimicrob. Chemother. 52 (2003) 450–456, https://doi.org/10.1093/jac/dkg355.
[57] M. Oh, H. Lee, S. Kim, B. Kim, G.S. Song, J.-G. Shin, J.-L. Ghim, Evaluation of pharmacokinetic drug-drug interaction between tegoprazan and clarithromycin in healthy subjects, Transl. Clin. Pharm. 31 (2023) 114–123, https://doi.org/10.12793/tcp.2023.31.e11.
[58] G.M. Pacifici, Clinical pharmacology of clarithromycin, Biomed. J. Sci. Tech. Res 55 (2024) 47435–47445, https://doi.org/10.26717/BJSTR.2024.55.008762.
[59] A. El Harchi, A.S. Butler, Y. Zhang, C.E. Dempsey, J.C. Hancox, The macrolide drug erythromycin does not protect the hERG channel from inhibition by thioridazine and terfenadine, Physiol. Rep. 8 (2020) e14385, https://doi.org/10.14814/phy2.14385.